Probing the Fermi Energy Level and the Density of States Distribution in PbTe Nanocrystal (Quantum Dot) Solids by Temperature-Dependent Thermopower Measurements

Dong-Kyun Ko[†] and Christopher B. Murray[†,‡,*]

[†]Department of Materials Science and Engineering, University of Pennsylvania, 3231 Walnut Street, Philadelphia, Pennsylvania 19104, United States, and
[‡]Department of Chemistry, University of Pennsylvania, 231 S. 34th Street, Philadelphia, Pennsylvania 19104, United States

ABSTRACT The position of the Fermi energy level (E_F) with respect to the energy level where the transport process occurs (transport energy level, E_T) is an important parameter that determines the electrical properties of semiconductors. However, little attention has been devoted to investigating the position of E_F in semiconductor nanocrystal solids, both theoretically and experimentally. In this study, we perform temperature-dependent thermopower measurements on PbTe nanocrystal solids to directly probe $E_F - E_T$. We observe that as the size of the nanocrystals reduces, $E_F - E_T$ increases primarily due to the widening of density of state (DOS) gap. Furthermore, by modifying the monodispersity of nanocrystals, we observe an increase in thermopower as the distribution of energy states sharpens. This work promotes a deeper understanding of thermal occupation of energy states as well as electronic transport processes in semiconductor nanocrystal solid systems.

KEYWORDS: nanocrystal solids · thermopower · Fermi energy level · density of states · PbTe

The core of semiconductor technology is the ability to manipulate the electronic property of materials by introducing an electric field, light, impurity content, or by changing the temperature. Solids artificially constructed from semiconductor nanocrystals provide additional size-dependent functionalities and have generated enormous interest in device applications such as photodetectors,[1] transistors,[2] thermoelectrics,[3] and solar cells.[4,5] In this class of materials, as well as in bulk semiconductors, the position of the Fermi energy level (E_F) relative to the transport energy level (E_T) is a key parameter in determining the electronic property of the system. Currently, research is progressing to incorporate nanocrystal solids into more complex architectures, including metal–semiconductor junctions,[6,7] semiconductor heterojunctions,[8] and organic/inorganic hybrid structures.[9,10] However, there are a limited number of studies devoted to measuring and interpreting E_F in semiconductor nanocrystal solids,[11] which is crucial in optimizing device performance.

In this work, we directly extract $E_F - E_T$ by applying temperature-dependent thermopower measurements to semiconductor nanocrystal solids. This measurement technique is particularly useful for nanocrystal solid systems in which electron or hole conduction occurs *via* hopping between localized energy states[12,13] above or below the E_F, respectively. The electrical conductivity measurements cannot distinguish $E_F - E_T$ and the activation energy for mobility separately in these systems. Furthermore, thermopower measurements are conducted under open-circuit conditions, and it is insensitive to the contact resistance, which give us an additional advantage over electrical conductivity measurements. Using temperature-dependent thermopower measurements we extract each term of the thermopower equation[14] and examine their physical meaning as applied to semiconductor nanocrystal solids.

RESULTS AND DISCUSSION

The thermopower (α, Seebeck coefficient) is the heat carried per charge carrier divided by the temperature (μV/K), or in thermodynamic terms, the entropy transported per carrier. A general expression for thermopower of semiconductors (*p*-type) was derived by Fritzsche:[14]

$$\alpha = \frac{k}{e}\left[\frac{(E_F - E_T)}{kT} + A\right] \quad (1)$$

where, k is the Boltzmann constant, e is the elementary charge, and A is a temperature independent constant (heat of transport constant). Here we define the transport energy level E_T associated with the onset of mobility. Unlike bulk semiconductors, E_T in a nanocrystal

* Address correspondence to cbmurray@sas.upenn.edu, cbmurray@seas.upenn.edu.

Received for review February 25, 2011 and accepted April 20, 2011.

Published online April 20, 2011
10.1021/nn2007817

solid is not necessarily the edge of density of states (DOS). When a charge carrier is thermally excited to the very edge of the DOS, there is a low probability of finding a nearby energy state with the energy difference smaller than kT and thus the carriers remain immobile. As the carriers are excited to E_T, a continuous percolation path between two electrical contacts forms and the carrier starts to hop with a detectible mobility. Beyond E_T, the mobility increases abruptly with increasing available energy states for transport. As illustrated in Figure 1, the position of E_T may lie between the edge and the peak of the DOS depending on the monodispersity of nanocrystals, which determines the distribution of energy states. The first term in the bracket is known as the configurational entropy contribution to the thermopower[15−18] which is independent of the transport mechanism. It is related to the change in entropy of the system by thermally exciting n charge carriers across the DOS gap, and distributing them on N available states at the transport level. The same equation can be derived from the Boltzmann formula for the calculation of entropy of mixing (Heikes formula) and replacing the carrier concentration term using the Fermi−Dirac distribution function.[16] The second term A, known as the heat of transport constant, accounts for the carriers beyond E_T. It represents the additional kinetic energy of the carriers, in units of kT, weighted by their relative contribution to the total conductivity:

$$A = \frac{\int_{-\infty}^{0} \frac{\varepsilon}{kT}\sigma(\varepsilon)\,d\varepsilon}{\int_{-\infty}^{0} \sigma(\varepsilon)\,d\varepsilon}, \quad \varepsilon = E_T - E \qquad (2)$$

The heat of transport constant A depends on the energy-dependent conductivity $\sigma(E)$, which is a sensitive function of energy-dependent density of state $D(E)$ and mobility $\mu(E)$. In bulk semiconductors, the heat of transport constant is a small value between 1 and 2. In semiconductor nanocrystal solid systems, constant A can have a larger value ($A > 2$) if a wider distribution of energy states are utilized for transport. It is governed by the steepness of the rise of the $D(E)$ from E_T to the peak of the DOS, given that the width of the DOS distribution exceeds kT.[19,20]

Both the position of $E_F - E_T$ and the heat of transport constant A are extracted from the temperature-dependent thermopower measurements. The slope of thermopower *versus* $1/T$ gives the $E_F - E_T$ and from the y-intercept the constant A is derived. Practically, as shown in Figure 2a, when measuring thermopower at each temperature point set by the cooling stage, the applied temperature difference ΔT generated from the resistive heater should be small (~1.5 K). This is to ensure that the applied ΔT does not perturb the stage temperature. Accurate measurement of small thermovoltage (due to small ΔT) then may be hindered by other thermovoltages generated from wires,

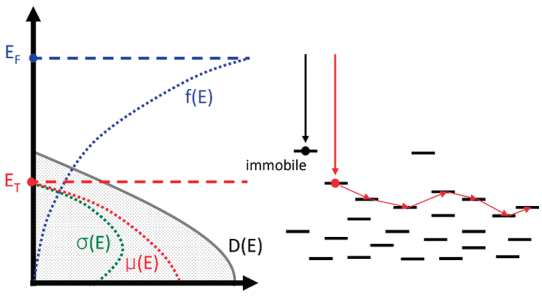

Figure 1. Schematic illustration of energy-dependent mobility, density of state, and Fermi−Dirac distribution function showing energy-dependent conductivity in *p*-type semiconductor nanocrystal solids. Transport energy level E_T is defined as an energy level where the hopping mobility increases from zero. In a physical picture, it is the lowest energy level where the percolation path of energy state emerges between two contacts.

connectors, and instrument electronics. These normally contribute as major sources of error. These errors can be eliminated by taking two measurements at different heater power outputs,[21] as shown in Figure 2b. The measured open-circuit voltage V_{oc} of the sample and the reference voltage V_{ref} of a constantan at two different heater outputs (P_1 and P_2) are

$$\begin{aligned} V_{oc}(P_1) &= \alpha_{sam}\Delta T(P_1) + \Delta V_{error}^{sam} \\ V_{ref}(P_1) &= \alpha_{ref}\Delta T(P_1) + \Delta V_{error}^{ref} \\ V_{oc}(P_2) &= \alpha_{sam}\Delta T(P_2) + \Delta V_{error}^{sam} \\ V_{ref}(P_2) &= \alpha_{ref}\Delta T(P_2) + \Delta V_{error}^{ref} \end{aligned} \qquad (3)$$

where, α_{sam} is the thermopower (Seebeck coefficient) of the sample and α_{ref} is the thermopower of reference constantan. The error voltages arising from sample measurement ΔV_{error}^{sam} and the reference measurement ΔV_{error}^{ref} is constant for two power outputs since the heat is applied only in proximity to the sample and constantan junction, as shown in Figure 2a. With the elimination of ΔV_{error}^{sam} and ΔV_{error}^{ref} by taking the difference of the two voltage measurements, an accurate value of the sample's thermopower is obtained:

$$\alpha_{sam} = \alpha_{const}\frac{[V_{oc}(P_1) - V_{oc}(P_2)]}{[V_{ref}(P_1) - V_{ref}(P_2)]} \qquad (4)$$

A typical plot of V_{oc} *versus* ΔT (while the stage temperature is fixed) for a PbTe nanocrystal solid (8.71 nm) is shown in Figure2c. The open circuit voltage V_{oc} is zero at the origin and the constant slope indicates that the thermopower of 856.37 μV/K is an inherent property of the solid. A typical temperature-dependent thermopower measurement, α_{sam} *versus* stage temperature T (while ΔT is fixed), is shown in Figure 2d. Reliable thermopower measurements were obtained from 300 to 190 K. Below 190 K the thermopower reading starts to fluctuate, in some cases to negative values. Interestingly, such behavior was similarly observed in liquid mercury near the critical point,[22,23] although the reason is not clearly known. At lower temperatures, the voltage measurement

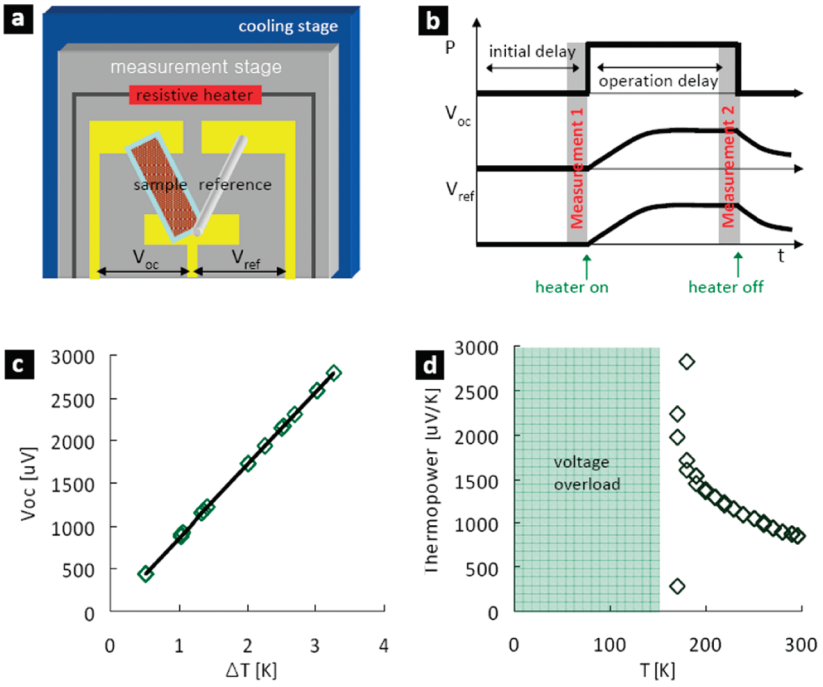

Figure 2. (a) Schematic diagram of temperature-dependent thermopower measurement configuration. (b) Plot of resistive heater power output, open-circuit voltage V_{oc} of the sample, and reference voltage V_{ref} of constantan as a function of time, showing a data collection scheme for a current thermopower measurement system. (c) Measurements of open-circuit voltages on a PbTe nanocrystal (8.71 nm) solid as a function of applied temperature difference ΔT while the temperature of the cooling stage was fixed at room temperature. The slope gives the thermopower of 856.37 μV/K. (d) Plot of temperature-dependent thermopower measurement on the same sample while ΔT was fixed at 1.5 K. Around ~180 K the thermopower starts to fluctuate and below 170 K the measurement readings were unreliable due to voltage overload.

reaches maximum overload due to the high resistance of the sample.

Our first interest in this work is to examine $E_F - E_T$ as a function of PbTe nanocrystal size. A series of nanocrystals with different sizes varying from 6.4 to 11.5 nm were synthesized by modifying the reaction temperature, time, and Pb/Te ratio, as shown in Figure 3. Average nanocrystal size and size distribution were characterized using small-angle X-ray scattering (SAXS) and were compared with the transmission electron microscopy (TEM) data. SAXS data curves were fit using a standard spherical model with a Schultz distribution function accounting for the nanocrystal size distributions.[24−26] Average size determined from TEM image analysis compared with SAXS data fitting show an increasing deviation as the nanocrystal size increases. This increase in error is due to the evolution of shape from spherical to cubic as the PbTe nanocrystals grow.[27−30] This is shown in Figure 3a for the largest PbTe nanocrystal which explains the discrepancy of average size determination using spherical SAXS fitting model. The average size and distribution, expressed in standard deviation, determined by SAXS experiments were 11.5 nm ± 8.1% (largest nanocrystals, denoted as A), 9.97 nm ± 10.8% (B), 8.71 nm ± 9.3% (C), 7.55 nm ± 9.5% (D), and 6.4 nm ± 11.4% (smallest nanocrystals, E).

The optical absorption spectra of PbTe nanocrystals are shown in Figure 4a. From the largest (A) to the smallest (E) nanocrystals, optical gaps defined from the first excitonic peaks were 0.54, 0.60, 0.67, 0.74, and 0.82 eV. Corresponding temperature-dependent thermopower measurements are shown in Figure 4b. For all, the samples were dropcast and treated with 1 M of hydrazine (**NOTE: hydrazine is toxic by vapor inhalation and skin absorption**) in anhydrous acetonitrile overnight followed by subsequent cycles of nanocrystal depositions and hydrazine treatments to make a continuous thick film. The samples were mounted on the cooling stage in a closed chamber which was kept under vacuum (6 mTorr) for 3 h prior to the measurements. Hydrazine treatment[27,31,32] is known to reduce the interparticle spacing facilitating interparticle carrier transport and to dope PbTe nanocrystal solids *n*-type. Under vacuum conditions, hydrazine desorbs from the surface of nanocrystals converting the solid to *p*-type[31] (for the measurement consistency, see details in the Supporting Information). All samples, sizes ranging from A to E, show positive thermopower indicating that the majority carriers responsible for electronic conduction are holes. This is consistent with the result that only holes can be accumulated in the field-effect transistor measurements (see details in the Supporting Information), suggesting that PbTe nanocrystal solids can be described as unipolar *p*-type semiconductors. The slopes of each sample from the linear fit give 239.81 ± 1.36 meV (A), 284.47 ± 0.95 meV (B), 337.38 ± 5.75 meV (C), 373.74 ± 3.25 meV (D), and 423.7 ± 6.16 meV (E)

from the largest to the smallest samples, respectively. Comparison of the optical gap and the temperature dependent thermopower measured on nanocrystal sample A, indicates that $E_F - E_T$ is smaller than half of the measured optical gap. This indicates that E_F lies below the midgap. As the size of the constituent nanocrystals is reduced, the separation between the lowest occupied and the highest unoccupied energy states increases due to quantum confinement. This results in the DOS gap widening in the solid as illustrated in Figure 4c and reflected in the increasing slope ($E_F - E_T$) in Figure 4b. It is worth noting that the smallest nanocrystal samples exhibit the highest electrical resistivity (see details in the Supporting Information), which results in reduced accuracy of the thermopower measurement. This is observed in sample E of Figure 4b as the measured data fluctuate around the linear regression. While these temperature-dependent thermopower measurements cannot directly reveal the exact position of E_F and E_T, their difference ($E_F - E_T$) can be a valuable piece of information when combined with other material characterization techniques. First, if the effective density of state $D(E)$ is known, the carrier concentration can be calculated from the well-known Maxwell–Boltzmann statistics ($p = D(E)\exp[(E_F - E_T)/kT]$). Second, the exact position of the Fermi energy level can be determined with either electron affinity or ionization potential information (with respect to the zero vacuum level), which can be measured by cyclic voltammetry[33] or ultraviolet photoemission spectroscopy (UPS).[34] Full DOS diagram for semiconductor nanocrystal solids can be constructed to estimate the electrostatic potential (corresponding to band-bending in bulk semiconductors) created at the semiconductor–semiconductor or metal–semiconductor junctions. Finally, in material systems where E_T is fixed, the temperature-dependent thermopower alone can be a powerful tool to monitor the shift in E_F as a function of doping. This was previously studied in a system where PbTe nanocrystals serve as a semiconductor matrix (thus, E_T is fixed) and different concentrations of Ag_2Te nanocrystals were introduced replacing PbTe

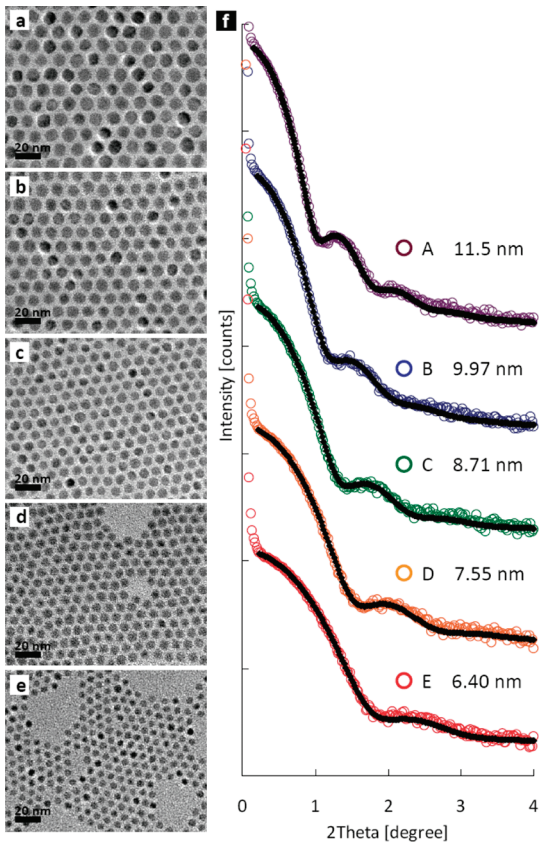

Figure 3. TEM image of PbTe nanocrystals synthesized with five different sizes (a–e) and corresponding SAXS curves (f). The scattering curves were fit (shown in solid line) using a spherical model with particle size distribution corresponding to the Schultz distribution function. Largest nanocrystals (a and purple scattering curve A in panel f) yields an average size of 11.5 nm with 8.1% standard deviation. Smallest nanocrystals had average size of 6.4 nm with a standard deviation of 11.4% (e and red curve E in panel f). Medium size range particles (b–d) denoted as curves B, C, and D in panel f show average sizes and distributions of 9.97 nm ± 10.8%, 8.71 nm ± 9.3%, and 7.55 nm ± 9.5%, respectively.

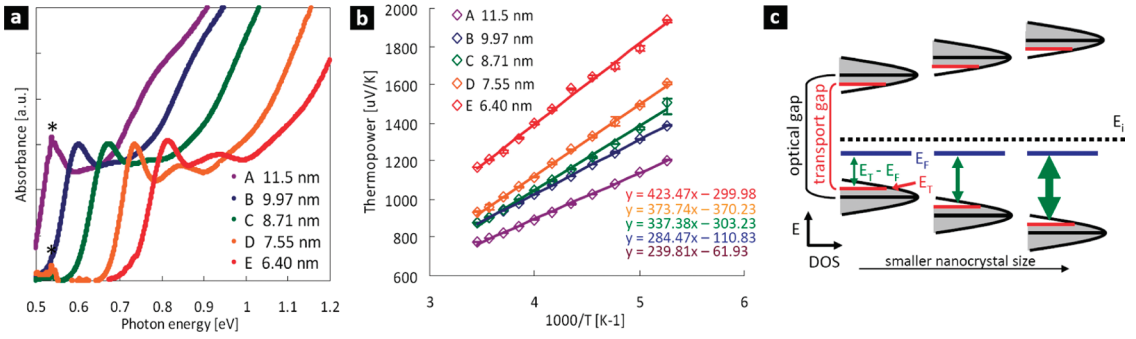

Figure 4. (a) Optical absorption spectra of PbTe nanocrystals of five different sizes. Two asterisks indicate superimposition of solvent (squalane) and surfactant (oleic acid) absorption peak. (b) Temperature-dependent thermopower measurements on nanocrystal solids constructed from various sizes of PbTe nanocrystals. Each solid line is a linear fit to extract slopes which reveal $E_F - E_T$. The *y*-intercept comes from three different contributions which include the heat of transport constant. (c) Schematic illustration of $E_F - E_T$ as a function of nanocrystal size as measured in temperature-dependent thermopower measurements.

nanocrystals as substitutional dopants.[11] The position of E_T as well as E_F may also show temperature dependent shifts. However, the shifts in these energy levels do not affect the slope of temperature-dependent thermopower, which will be discussed below in the analysis of the *y*-intercept.

The *y*-intercepts extracted from the thermopower plots are −61.93 ± 5.81 (A), −110.83 ± 4.07 (B), −303.23 ± 24.62 (C), −370.23 ± 13.90 (D), and −299.98 ± 26.37 mV/K (E), from largest to smallest nanocrystals, respectively. There are three contributing factors to the *y*-intercept. The first is the heat of transport constant *A*, which is determined by energy-dependent conductivity $\sigma(E)$. For the case where $D(E)$ and $\mu(E)$ increases as $(E_T - E)^m$, the theoretical prediction[14,20,35] estimates $A = 1 + m$. The heat of transport constant for PbTe nanocrystal solids within the monodispersity range mentioned above is expected to be around 3 based on the curvature of the optical DOS in Figure 4a (see details in the Supporting Information). The second factor is attributed to the variation in DOS gap (and thus E_T) as a function of temperature.[36−39] Assuming a linear relationship and replacing $E_F - E_T$ term by $E_F - (E_T + \gamma_g T)$ in eq 2 gives

$$\alpha = \frac{k}{e}\left[\frac{(E_F - E_T)}{kT} - \frac{\gamma_g}{k} + A\right] \quad (5)$$

where, γ_g is temperature-dependent DOS gap coefficient. The magnitude as well as the sign of this coefficient is known to have a size dependence,[40,41] which can deviate from the bulk value.[42,43] Although the exact value is unknown, in the size range of 6.4−11.5 nm, our measurements suggest that PbTe nanocrystals may have large temperature coefficients (γ_g > 370 meV/K). This factor contributes to the negative *y*-intercept of the temperature-dependent thermopower plot, since it is physically impossible for the heat of transport constant to have a negative value. As the nanocrystal size in the solids reduces, the relaxation of quantum confinement due to expansion of crystallite size and the electron−phonon coupling term dominates the contribution from the thermal expansion of lattice,[41] shifting the $-\gamma_g/k$ term more negative. Thus, for smaller nanocrystal sizes, the *y*-intercept shows more negative value. The third factor comes from the shift in E_F,[35,44−46] which gives a positive contribution to the *y*-intercept. In nanocrystal solids, various surface and nonstoichiometric defects may introduce additional energy states near the midgap[47] which can be asymmetrically distributed throughout the DOS gap. At 0 K, the Fermi energy may lie below the midgap if more defect states are distributed below the DOS center. Increasing the temperature shifts the Fermi level toward the midgap as the intrinsic carrier dominates the position of the E_F. This effect will predominate in narrow DOS gap nanocrystal solids, which is exhibited as an increasing value in the *y*-intercept as the size of the nanocrystal increases. Taking the E_F shift into account $((E_F + \gamma_F T) - E_T)$, the following equation

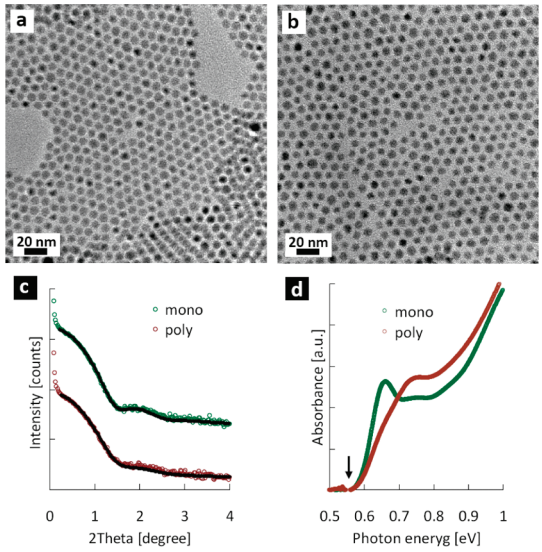

Figure 5. TEM image of (a) monodisperse and (b) polydisperse PbTe nanocrystals. (c) Fitting scattering profiles (shown in solid line) indicate that monodisperse nanocrystals have average size and distribution of 7.77 nm ± 9.6% and 7.45 nm ± 14.3% for polydisperse nanocrystals. (d) Corresponding absorption spectra for two samples. Arrow indicates the common edge of optical DOS.

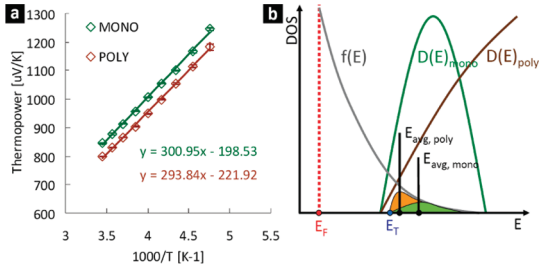

Figure 6. (a) Temperature-dependent thermopower measurements performed on both monodisperse and polydisperse nanocrystal solids. The *y*-intercept of the linear fit is higher in monodisperse nanocrystal solids due to the increase in heat of transport constant. (b) Schematic diagram (not to scale) of carrier distribution in monodisperse and polydisperse nanocrystal solid to estimate the average kinetic energy and the heat of transport constant.

summarizes the *y*-intercept of the temperature-dependent thermopower:

$$\alpha = \frac{k}{e}\left[\frac{(E_F - E_T)}{kT} - \frac{\gamma_g}{k} + \frac{\gamma_F}{k} + A\right] \quad (6)$$

To study the effect of the DOS on the heat of transport constant in detail, samples were prepared such that the edge of the DOS was kept constant and the distance between the DOS edge and the peak was varied by increasing the polydispersity of nanocrystals. As shown in Figure 5a−c the TEM image of the nanocrystals and the SAXS profiles indicate two distinct monodisperse (denoted as mono) and polydisperse (poly) nanocrystal samples. Optical absorption measurements (Figure 5d) show a wider distribution in the first excitonic transition peak for the polydisperse samples but with a common

optical DOS edge. Increasing the polydispersity by 50% (as confirmed from SAXS data in Figure 5c) showed negligible change in $E_F - E_T$ as shown by the similar slope in Figure 6a, and the average size of the nanocrystals only decreased by 0.32 nm. The larger *y*-intercept of the temperature-dependent thermopower plots observed in the monodisperse nanocrystal solid can be attributed to a higher heat of transport constant (since other parameters are fixed). The increase in heat of transport constant can be understood by estimating the distribution of mobile carriers inside the DOS and predicting the average kinetic energy. This is conducted by multiplying the Fermi distribution function with $D(E)$ and taking the average of the distribution. From Figure 6b, the distance between E_T and the average kinetic energy of carriers E_{avg} is larger in monodisperse nanocrystal solid. Although the contribution from $\mu(E)$ may also increase the *y*-intercept, it is expected that a sharper distribution of the DOS shifts the average kinetic energy further away from the E_T, thereby increasing the heat of transport constant in the current study. Sharp peaks in DOS have been theoretically[48−50] and experimentally[51,52] predicted to increase thermopower. Nanocrystal solids inherently possess sharp DOS compared to that of the bulk counterpart. In nondegenerate PbTe nanocrystal solids, current analysis reveals that sharp distribution of DOS increases the heat of transport constant *A*, thereby increasing the thermopower. This study provides a general strategy for maximizing the thermoelectricity in materials composed of nanocrystals. Minimizing the size distribution of the nanocrystals sharpens the DOS peak, which is expected to increase not only the thermopower, but also the electrical conductivity, by reducing energy level variations. This, in turn, maximizes thermoelectric power factor ($\alpha^2\sigma$) of semiconductor nanocrystal solid systems (with a given carrier concentration).

CONCLUSION

The purpose of this study was to apply temperature-dependent thermopower measurements on nanocrystal solids to investigate $E_F - E_T$ and heat of transport constant *A*. By varying the size of the nanocrystals in a solid we have examined the change in $E_F - E_T$, which was primarily due to the change in DOS gap. Furthermore, the change in *y*-intercept of temperature-dependent thermopower plot as a function of nanocrystal size as well as monodispersity enabled us to study additional terms reflecting the electronic structure and property of nanocrystal solids and to explore a strong dependence of heat of transport constant on DOS distribution. Most of the studies on nanocrystal solids to date have focused on the introduction of electric fields or light to investigate charge carrier transport properties. Electrons and holes, however, are not only charge carriers, but also heat carriers. Therefore, by applying external heat, thermopower measurements can provide a unique perspective on carrier transport studies in nanocrystal solid systems.

METHODS

Synthesis and Characterization. PbTe nanocrystals were synthesized using a similar procedure reported previously.[27] In a typical synthesis, 1.138 g of lead acetate trihydrate (Aldrich, 99%) and 2 mL of oleic acid (Aldrich, 90%) was added into 20 mL of squalane (Aldrich, 99%) which was heated at 100 °C for 2 h under vacuum. After the solution was heated to 185 °C under nitrogen flow, 4 mL of trioctylphosphine telluride (0.75M, TOP-Te) solution, which was prepared by dissolving 4.75 g of tellurium shot in 50 mL of trioctylphosphine (Aldrich, 90%), was injected, and the growth temperature was maintained at 175 °C. The growth time was varied from 20 s to 2 min 30 s which yielded nanocrystal sizes varying from 6.4 nm (E) to 9.97 nm (B). For the largest 11.5 nm nanocrystals (A), 6 mL of TOP-Te was injected at 195 °C and the growth was maintained at 180 °C for 2 min and 30 s. Polydisperse nanocrystals were synthesized by injecting 4 mL of TOP-Te slowly in a dropwise manner at 185 °C where the growth temperature dropped down to 173 °C gradually during 1 min and 15 s reaction. All syntheses were performed using the standard air-free technique, and separation and purification processes were done in a nitrogen glovebox using anhydrous hexane and acetone. Optical absorption measurements on PbTe nanocrystals dissolved in tetrachloroethylene (Aldrich, 99%) were performed using Analytical Spectral Devices QSP 350-2000 with airtight cuvettes. TEM images were obtained using JEOL 1400. For SAXS experiments, samples were prepared in sealed capillaries filled with PbTe nanocrystals dissolved in hexane, and the measurements were conducted using Rigaku Smartlab high-resolution diffractometer.

Sample Preparation and Measurements. Samples for thermopower measurements were prepared inside the nitrogen glovebox without exposure to oxygen and moisture. PbTe nanocrystals, dissolved in anhydrous hexane and octane mixture, were drop-cast on thin microscope cover glass to prepare a glassy film as described in a previous report.[11] This cover glass was scribed beforehand with precision diamond scriber so that small rectangular shapes can be easily cleaved later on with a small amount of pressure. PbTe nanocrystal film was then submerged in 1 M of hydrazine (Aldrich, anhydrous, 98%) in acetonitrile (Aldrich, anhydrous, 99.8%) overnight. Several depositions and treatments were repeated to fill in the cracks formed in the film, and a small rectangle portion was removed from the cover glass. All samples were prepared in approximately 1.5 mm × 4 mm geometry with an average 85 ± 20 nm nanocrystal film thickness (SEM cross-section, FEI Strata DB235) and were mounted on the measurement stage using silver paste (Leitsilber 200, Ted Pella). Temperature-dependent thermopower measurements were conducted using MMR technologies K-20 and SB-100 with a high impedance amplifier (100 gain). Copper-constantan (alloy of 45% nickel and 55% copper) is used as a reference junction to monitor temperature difference ΔT. Throughout the measurement, heater power output was adjusted so that ΔT was fixed at 1.5 K, initial delay was set to 5 min for the temperature of the sample to reach equilibrium with the cooling stage, and operation delay was adjusted to 30 s in order to achieve steady state across the measurement stage. All samples were kept at 6 mTorr for 3 h prior to the measurements.

Acknowledgment. This work was supported in part by National Science Foundation though PENN MRSEC DMR-0520020 enabling structural characterization and analysis of all experiment results. Partial support was provided by U.S. Department

of Energy, Office of Basic Energy Sciences, Division of Materials Sciences and Engineering under Award No. DE-SC0002158 (C.B.M. and D.-K.K.) enabling the synthesis of materials. C.B.M. thanks Richard Perry University Professorship for support of his supervisor role.

Supporting Information Available: Table summarizing the basic physical properties of the samples prepared for the temperature-dependent thermopower experiments and the measurement analyses, consistency of thermopower measurements, estimation of heat of transport constant from the curvature of the optical DOS, field-effect transistor characteristics on both hydrazine treated and vacuum pulled PbTe nanocrystal solids. This material is available free of charge *via* the Internet at http://pubs.acs.org.

REFERENCES AND NOTES

1. Konstantatos, G.; Howard, I.; Fischer, A.; Hoogland, S.; Clifford, J.; Klem, E.; Levina, L.; Sargent, E. H. Ultrasensitive Solution-Cast Quantum Dot Photodetectors. *Nature* **2006**, *442*, 180–183.
2. Kang, M. S.; Lee, J.; Norris, D. J.; Frisbie, C. D. High Carrier Densities Achieved at Low Voltages in Ambipolar PbSe Nanocrystal Thin-Film Transistors. *Nano Lett.* **2009**, *9*, 3848–3852.
3. Wang, R. Y.; Fesser, J.; Lee, J. -S.; Talapin, D. V.; Segalman, R.; Majumdar, A. Enhanced Thermopower in PbSe Nanocrystal Quantum Dot Superlattices. *Nano Lett.* **2008**, *8*, 2283–2288.
4. Beard, M. C.; Hillhouse, H. W. Solar Cells from Colloidal Nanocrystals: Fundamentals, Materials, Devices, and Economics. *Curr. Opin. Colloid. In.* **2009**, *14*, 245–259.
5. Nozik, A. J. Quantum Dot Solar Cells. *Phys. E* **2002**, *14*, 115–120.
6. Luther, J. M.; Law, M.; Beard, M. C.; Song, Q.; Reese, M. O.; Ellingson, R. J.; Nozik, A. J. Schottky Solar Cells Based on Colloidal Nanocrystal Films. *Nano Lett.* **2008**, *8*, 3488–3492.
7. Gur, I.; Fromer, N. A.; Geier, M. L.; Alivisatos, A. P. Air-Stable All-Inorganic Nanocrystal Solar Cells Processed from Solution. *Science* **2005**, *310*, 462–465.
8. Sun, B.; Findikoglu, A. T.; Sykora, M.; Werder, D. J.; Klimov, V. I. Hybrid Photovoltaic Based on Semiconductor Nanocrystals and Amorphous Silicon. *Nano Lett.* **2009**, *9*, 1235–1241.
9. Greenham, N. C.; Peng, X.; Alivisatos, A. P. Charge Separation and Transport in Conjugated-Polymer/Semiconductor-Nanocrystal Composites Studied by Photoluminescence Quenching and Photoconductivity. *Phys. Rev. B* **1996**, *54*, 17628–17637.
10. Arango, A. C.; Oertel, D. C.; Xu, Y.; Bawendi, M. G. Heterojunction Photovoltaics Using Printed Colloidal Quantum Dots as a Photosensitive Layer. *Nano Lett.* **2009**, *9*, 860–863.
11. Ko, D.-K.; Urban, J. J.; Murray, C. B. Carrier Distribution and Dynamics of Nanocrystal Solids Doped with Artificial Atoms. *Nano Lett.* **2010**, *10*, 1842–1847.
12. Chandler, R. E; Houtepen, A. J.; Nelson, J.; Vanmaekelbergh, D. Electron Transport in Quantum Dot Solids: Monte Carlo Simulations of the Effects of Shell Filling, Coulomb Repulsion, and Site Disorder. *Phys. Rev. B* **2007**, *75*, 085325.
13. Van de Lagemaat, J. Einstein Relation for Electron Diffusion on Arrays of Weakly Coupled Quantum Dots. *Phys. Rev. B* **2005**, *72*, 235319.
14. Fritzsche, H. A General Expression for the Thermoelectric Power. *Solid State Commun.* **1971**, *9*, 1813–1815.
15. Rowe, D. M. *Thermoelectrics Handbook: Macro to Nano*; CRC Press: Boca-Raton, FL, 2006.
16. Tilley, R. J. D. *Principles and Applications of Chemical Defects*; CRC Press: Boca-Raton, FL, 1998.
17. Wood, C.; Emin, D. Conduction Mechanism in Boron Carbide. *Phys. Rev. B* **1984**, *29*, 4582–4587.
18. von Mühlenen, A.; Errien, N.; Schaer, M.; Bussac, M. N.; Zuppiroli, L. Thermopower Measurements on Pentacene Transistors. *Phys. Rev. B* **2008**, *75*, 115338.
19. Emin, D. Thermoelectric Power Due to Electronic Hopping Motion. *Phys. Rev. Lett.* **1975**, *35*, 882–885.
20. Baily, S. A.; Emin, D. Transport Properties of Amorphous Antimony Telluride. *Phys. Rev. B* **2006**, *73*, 165211.
21. Resel, R; Gratz, E.; Burkov, A. T.; Nakama, T.; Higa, M.; Yagasaki, K. Thermopower Measurements in Magnetic Fields up to 17 T Using the Toggled Heating Method. *Rev. Sci. Instrum.* **1996**, *67*, 1970–1975.
22. Cusack, N. E.; Neale, F. E. Thermoelectric Power Near the Critical Point of Expanded Fluid Mercury. *J. Phys. F: Metal Phys.* **1979**, *9*, 85–94.
23. Yao, M.; Endo, H. Thermoelectric Power of Expanded Fluid Mercury and Dilute Amalgams. *J. Phys. Soc. Jpn.* **1982**, *51*, 1504–1509.
24. Brochert, H.; Shevchenko, E. V.; Robert, A.; Mekis, I.; Kornowski, A.; Grübel, G.; Weller, H. Determination of Nanocrystal Sizes: A Comparison of TEM, SAXS, and XRD Studies of Highly Monodisperse $CoPt_3$ Particles. *Langmuir* **2005**, *21*, 1931–1936.
25. Reiker, T.; Hanprasopwattana, A.; Datye, A.; Hubbard, P. Particle Size Distribution Inferred from Small-Angle X-ray Scattering and Transmission Electron Microscopy. *Langmuir* **1999**, *15*, 638–641.
26. Kotlarchyk, M.; Chen, S.-H. Analysis of Small Angle Neutron Scattering Spectra from Polydisperse Interacting Colloids. *J. Chem. Phys.* **1983**, *79*, 2461–2469.
27. Urban, J. J.; Talapin, D. V.; Shevchenko, E. V.; Murray, C. B. Self-Assembly of PbTe Quantum Dots into Nanocrystal Superlattices and Glassy Films. *J. Am. Chem. Soc.* **2006**, *128*, 3248–3255.
28. Murphy, J. E.; Beard, M. C.; Norman, A. G.; Ahrenkirl, S. P.; Johnson, J. C.; Yu, P.; Mićić, O. I.; Ellingson, R. J.; Nozik, A. J. PbTe Colloidal Nanocrystals: Synthesis, Characterization, and Multiple Exciton Generation. *J. Am. Chem. Soc.* **2006**, *128*, 3241–3247.
29. Mokari, T.; Zhang, M.; Yang, P. Shape, Size, and Assembly Control of PbTe Nanocrystals. *J. Am. Chem. Soc.* **2007**, *129*, 9864–9865.
30. Lu, W.; Fang, J.; Stokes, K. L.; Lin, J. Shape Evolution and Self Assembly of Monodisperse PbTe Nanocrystals. *J. Am. Chem. Soc.* **2004**, *126*, 11798–11799.
31. Talapin, D. V.; Murray, C. B. PbSe Nanocrystal Solids for n- and p-Channel Thin Film Field-Effect Transistors. *Science* **2005**, *310*, 86–89.
32. Law, M.; Luther, J. M.; Song, Q.; Hughes, B. K.; Perkins, C. L.; Nozik, A. J. Structural, Optical, and Electrical Properties of PbSe Nanocrystal Solids Treated Thermally or with Simple Amines. *J. Am. Chem. Soc.* **2008**, *130*, 5974–5985.
33. Kucur, E.; Riegler, J.; Urban, G. A.; Nann, T. Determination of Quantum Confinement in CdSe Nanocrystals by Cyclic Voltammetry. *J. Chem. Phys.* **2003**, *119*, 2333–2337.
34. Colvin, V. L.; Alivisatos, A. P. Valence-Band Photoemission from a Quantum-Dot System. *Phys. Rev. Lett.* **1991**, *66*, 2786–2789.
35. Jones, Di. I.; Le Comber, P. G.; Spear, W. E. Thermoelectric Power in Phosphorous Doped Amorphous Silicon. *Philos. Mag.* **1977**, *36*, 541–551.
36. Emim, D. Effect of Temperature-Dependent Band Shifts on Semiconductor Transport Properties. *Solid State Commun.* **1977**, *22*, 409–411.
37. Edmond, J. T. Electronic Conduction in As_2Se_3, As_2Se_2Te, and Similar Materials. *Brit. J. Appl. Phys.* **1966**, *17*, 979–989.
38. Mahadevan, S.; Rao, K. J. Thermoelectric Power of As-Se-Te Glasses. *J. Non-Cryst. Solids* **1979**, *34*, 53–62.
39. Moustakas, T. D.; Weiser, K; Grant, A. J. Anomalous Thermoelectric Power of Some Liquid Chalcogenide Systems. *Solid State Commum.* **1975**, *16*, 575–579.
40. Olkhovets, A.; Hsu, R. -C.; Lipovskii, A.; Wise, F. W. Size-Dependent Temperature Variation of the Energy Gap in Lead-Salt Quantum Dots. *Phys. Rev. Lett.* **1998**, *81*, 3539–3542.
41. Dai, Q.; Zhang, Y.; Wang, Y.; Hu, M. Z.; Zou, B.; Wang, Y.; Yu, W. W. Size-Dependent Temperature Effects on PbSe Nanocrystals. *Langmuir* **2010**, *26*, 11435–11440.

42. Baleva, M.; Georgiev, T.; Lashkarev, G. On the Temperature Dependence of the Energy Gap in PbSe and PbTe. *J. Phys.: Condens. Matter* **1990**, *2*, 2935–2940.
43. Keffer, C.; Hayes, T. M.; Bienenstock, A. Debye–Waller Factors and the PbTe Band-Gap Temperature Dependence. *Phys. Rev. B* **1970**, *2*, 1966–1976.
44. Elliott, E. R. *Physics of Amorphous Materials*; Longman Scientific & Technical: Harlow, Essex, England, 1990.
45. Spear, W. E. Doped Amorphous Semiconductors. *Adv. Phys.* **1977**, *26*, 811–845.
46. Beyer, W.; Medeišis, A.; Mell, H. Unusual Temperature Dependence of the Thermoelectric Power of Phosphorous-Doped Amorphous Silicon. *Commun. Phys.* **1977**, *2*, 121–125.
47. Hoang, K; Mahanti, S. D.; Jena, P. Theoretical Study of Deep-Defect States in Bulk PbTe and in Thin Films. *Phys. Rev. B* **2007**, *76*, 115432.
48. Hicks, L. D.; Dresselhaus, M. S. Thermoelectric Figure of Merit of a One-Dimensional Conductor. *Phys. Rev. B* **1993**, *47*, 16631.
49. Mahan, G. D.; Sofo, J. O. The Best Thermoelectric. *Proc. Natl. Acad. Sci. U.S.A.* **1996**, *93*, 7436–7439.
50. Shakouri, A. Thermoelectric, Thermionic, Thermophotovoltaic Energy Conversion. *Int. Conf. Thermoelect.* **2005**, 492–497.
51. Heremans, J. P.; Jovovic, V.; Toberer, E. S.; Saramat, A.; Kurosaki, K.; Charoenphakdee, A.; Yamanaka, S.; Snyder, G. J. Enhancement of Thermoelectric Efficiency in PbTe by Distortion of the Electronic Density of States. *Science* **2008**, *321*, 554–557.
52. Heremans, J.; Thrush, C. M. Thermoelectric Power of Bismuth Nanowires. *Phys. Rev. B* **1999**, *59*, 12579–12583.